

Hazard Assessment Comparison of Tazhiping Landslide Before and After Treatment **using finite volume method**

Dong Huang¹, **YuanJun Jiang^{1*}**, JianPing Qiao¹, Meng Wang¹

1. Key Laboratory of Mountain hazards and Surface process, Institute of Mountain hazards and Environment, Chinese Academy of Science, Chengdu 610041, China

*Corresponding author (yuanjun.jiang.civil@gmail.com).

Abstract: Through investigation and analysis of geological conditions and mechanical parameters of the Tazhiping landslide, the finite volume method was adopted, and, the rheological model was adopted to simulate the landslide and avalanche entire mass movement process. The present paper adopted **the numerical approach in RAMMS and** the GIS platform to simulate the mass movement process before and after treatment. This paper also provided the conditions and characteristic parameters of soil deposits (**thickness** flow height, **speed** velocity, and stresses) during the landslide mass movement process and mapped the 3D division of hazard zones before and after landslide treatment. Results indicated that the scope of hazard zones contracted after engineering treatment of the landslide. The extent of high-hazard zones was reduced by about 2/3 of the area before treatment, and characteristic parameters of the mass movement process after treatment decreased to 1/3 of those before treatment. Despite engineering treatment, the Tazhiping landslide still poses significant hazard to nearby settlements. Therefore, we propose that houses located in high-hazard zones be relocated or reinforced for protection.

Keywords: finite volume method; rheological model; motion feature parameters; hazard assessment

1. Introduction

The hazards of a landslide include scope of influence (i.e., source area, possible path area, and backward and lateral expansion area) and secondary disasters (i.e., reservoir surge, blast, and landslide-induced barrier lake). A typical landslide hazard assessment aims to propose a systematic hazard assessment method with regard to a given position or a potential landslide. Current research on typical landslide hazard assessment remains immature, and there are multiple methods for interpreting landslide hazards. To be specific, the scope of influence prediction of a landslide refers to deformation and instability characteristics such as sliding distance, movement speed, and bulking thickness range. The movement behavior of a landslide mass is related to its occurrence, sliding mechanisms, mass characteristics, sliding path, and many other factors. Current landslide movement prediction methods include empirical prediction and numerical simulation.

Empirical prediction method: The empirical prediction method involves

44 analyzing landslide flow through the collection of landslide parameters in the field. It
45 further consists of the geomorphologic method (Costa, 1984; Jackson et al., 1987;
46 Scott et al., 1993), the geometric change method (~~Zhang et al., 1994-1993~~; Finlay et
47 al., 1999; Michael-Leiba et al., 2003), and the volume change method (Fannin et al.,
48 2001). Empirical models are commonly simple and easy to apply, and the required
49 data are easy to obtain as well. **Numerical simulation method:** Numerical simulation
50 methods are further divided into the continuous deformation analysis method (Hung
51 1995; Evans et al., 2009; ~~Zhang .Y, 2013~~; Wang-L, et al., 2016), the discontinuous
52 deformation analysis method (Shi-G.H, 1988; ~~Yin et al., 2002~~), and the simplified
53 analytical simulation method (Christen et al., 2010a; Sassa, 2010; Bartelt et al., 2012;
54 Du et al., 2015). The numerical simulation method expresses continuous physical
55 variables using the original spatial and temporal coordinates with geometric values of
56 discrete points. Numerical simulations follow certain rules to establish an algebraic
57 equation set in order to obtain approximate solutions for physical variables.

58 Empirical prediction models only provide a simple prediction of the sliding path.
59 Due to the differences in geological environments, empirical prediction models
60 commonly have low generality. The continuous deformation method has the
61 advantage of an extremely strong replication capability, but it is not recommended
62 when analyzing ~~flow-type~~ ~~landslides-debris flows~~, lahars, or debris flows because of
63 complicated rheological behaviors (~~Iverson et al., 1997, 2001~~; ~~Hung et al., 2001~~;
64 ~~Portilla et al., 2010~~; ~~Chen et al., 2014~~). The fluid mechanics-based discontinuous
65 deformation method has several shortcomings such as, great computational burden,
66 difficult parameter selection, and difficult 3D implementation. The simplified
67 analytical simulation method fully takes into account the flow state properties of
68 landslides before introducing a rheological model and can easily realize 3D
69 implementation on the GIS platform. On that account, this paper adopted the
70 continuous fluid mechanics-based finite volume method (simplified analytical
71 simulation method). We introduce a rheological model on the basis of using mass as
72 well as momentum and energy conservation to describe the movement of landslides.
73 We also employed GIS analysis to simulate the entire movement process of Taziping
74 landslide and map the 2D division of hazard zones.

75

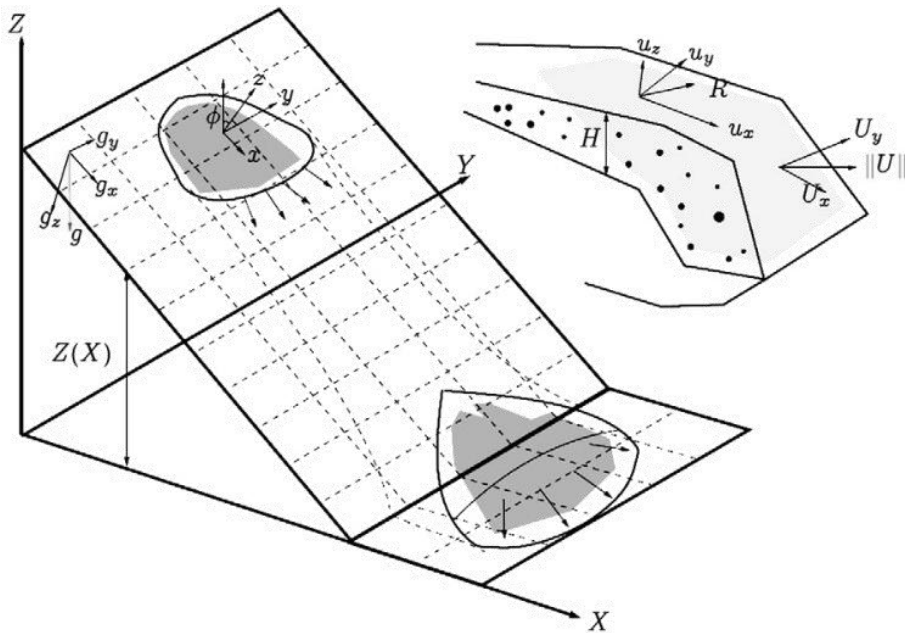
76 **2. Methods**

77 **2.1 Kinetic analysis method**

78 Adopting the continuous fluid mechanics-based finite volume method, this paper
79 took into account erosion action on the lower surface of the sliding mass and the
80 change in frictional resistance within the landslide-debris flow in order to establish a
81 computational model. The basic idea is to divide the calculation area into a series of
82 non-repetitive control volumes, ensuring that there is a control volume around each
83 grid point. Each control volume is then integrated by the unresolved differential
84 equation in order to obtain a set of discrete equations. The unknown variable is the
85 numerical value of the dependent variable at each grid point. To solve the integral of a
86 control volume, we make a hypothesis about the change rule of values among grid

87 points, that is, about their piecewise distribution profile. The finite volume method
 88 can satisfactorily overcome the finite element method's weakness of slow calculation,
 89 and solve the problem of complex region processing. Thus, we adopted the finite
 90 volume method to establish the kinematic model for the landslide flow process.

91 The core of the finite volume method is domain discretization. The finite volume
 92 method uses discrete points as a substitute for continuous space. The physical
 93 meaning of the discrete equation is the conservation of the dependent variable in a
 94 finite control volume. Establishment of the conservation equation is based on the
 95 continuous movement model, that is, the continuity hypothesis about landslide
 96 substances. We divided the landslide mass into a series of units and made the
 97 hypothesis that each unit has consistent kinematic parameters (speed at a depth,
 98 density, etc.) and physical parameters (Fig.1). We also established an Eulerian
 99 coordinate system-based conservation equation with regard to each control volume.



100

101 Fig.1 Schematic diagram of finite volume discretization (Christen et al., 2010a).

102

2.2 Control equation

103

The computational domain is defined as directions x and y , and the
 104 topographic elevation is given the coordinate $z(x, y)$. $H(x, y, t)$ is assumed as the

105

change relationship of landslide thickness with time; $U_x(x, y, t)$ and $U_y(x, y, t)$

106

respectively represent the mean movement speeds along directions x and y at

107

moment t ; $n_x = U_x / \sqrt{U_x^2 + U_y^2}$ and $n_y = U_y / \sqrt{U_x^2 + U_y^2}$ represent the cosinoidal and

108

sinusoidal flow vectors of the landslide on the plane $x - y$. The mean flow speed of

109 substances is defined as $U = \sqrt{U_x^2 + U_y^2}$.

110 Thus, the mass balance equation becomes:

$$111 \quad \partial_t H + \partial_x (HU_x) + \partial_y (HU_y) = \dot{Q} \quad (1)$$

112 wherein, $\dot{Q}(x, y, t)$ represents the change rate (entrainment rate) of landslide
113 volume with time.

114 Assuming that $l(x, y, t)$ represents the movement distance of the landslide with
115 time, we can obtain:

$$116 \quad \dot{Q} = \begin{cases} 0 & \text{if } h_i = 0 \\ \frac{\rho_i}{\rho_a} h_i \frac{U}{l} & \text{if } k_i l \geq h_i \\ \frac{\rho_i}{\rho_a} k_i U & \text{if } k_i l < h_i \end{cases} \quad (2)$$

117 wherein, h_i represents the thickness of the i th layer of the landslide in the
118 movement process; ρ_i represents the density of the i th layer of the landslide in the
119 movement process; ρ_a represents the density of the landslide; the dimensionless
120 parameter k_i represents the entrainment rate.

121 The momentum balance equation is:

$$122 \quad \partial_t (HU_x) + \partial_x (HU_x^2 + \frac{g_z k_{a/p} H^2}{2}) + \partial_y (HU_x U_y) = S_{gy} - S_f(R) [n_x] \quad (3)$$

$$123 \quad \partial_t (HU_y) + \partial_y (HU_y^2 + \frac{g_z k_{a/p} H^2}{2}) + \partial_x (HU_x U_y) = S_{gx} - S_f(R) [n_y] \quad (4)$$

124 wherein, $S_{gx} = g_x H$ and $S_{gy} = g_y H$ represent the dynamic components of the
125 acceleration of gravity in directions x and y ; $g = (g_x \ g_y \ g_z)$ represents the
126 vector of the acceleration of gravity; $k_{a/p}$ represents the pressure coefficient of soil;
127 ρ_a represents the density of the landslide; the dimensionless parameter k_i
128 represents the entrainment rate; $S_f(R)$ represents the frictional resistance.

129 The kinetic energy balance equation is:

$$130 \quad \partial_t (HR) + \partial_x (HRU_x) + \partial_y (HRU_y) = \dot{P} - \dot{D} \quad (5)$$

131 wherein, $R(x,y,t)$ represents the random mean kinetic energy of the landslide;
 132 $\dot{P}(x,y,t)$ and $\dot{D}(x,y,t)$ represent the random increased kinetic energy and decreased
 133 kinetic energy of the landslide.

134 2.3 Constitutive relationship

135 The improved Voellmy rheological model is applied in the computational
 136 simulation of the landslide. See the computational formula below:

$$137 \quad S_f = \frac{u_i}{\|U\|} (h\mu g_z + R_l U^2 + R_\zeta U^2) \quad (6)$$

$$138 \quad R_l = \mu h \frac{U^T K U}{U^2}, R_\zeta = \frac{g}{\zeta} \quad (7)$$

139 wherein, $u_i/\|U\|$ represents the unit vector in the movement direction of the
 140 landslide; μ represents the Coulomb friction coefficient, and is related to $R(x,y,t)$,
 141 the random mean kinetic energy of the landslide; R_l represents the gravity-related
 142 frictional force coefficient; K represents the substrate surface curvature; ζ
 143 represents the viscous friction coefficient of the ‘‘turbulent flow’’.

144 2.4 HLLE-Heun numerical solution

145 Synthesizing control equations (1), (3), (4) and (5), we can obtain the simplified
 146 form of the nonlinear hyperbola equation:

$$147 \quad \partial_t V + \nabla \cdot F(V) = G(V) \quad (8)$$

$$148 \quad V = \begin{pmatrix} H \\ HU_x \\ HU_y \\ HR \end{pmatrix} \quad G(V) := \begin{pmatrix} \dot{Q} \\ S_{gx} - S_{fx} \\ S_{gy} - S_{fy} \\ \dot{P} - \dot{D} \end{pmatrix}$$

$$149 \quad F(V) = \begin{pmatrix} HU_x & HU_y \\ HU_x^2 + g_z k_{alp} \frac{H^2}{2} & HU_x U_y \\ HU_x U_y & HU_y^2 + g_z k_{alp} \frac{H^2}{2} \\ HRU_x & HRU_y \end{pmatrix}$$

150 wherein, $V(x,y,t)$ represents a vector equation consisting of four unknown
 151 vector variables; $F(V)$ represents the flux function; $G(V)$ represents the source
 152 term. Based on the HLLE equation of the finite volume method and the quadrilateral
 153 grid, the node layout can adopt the grid center pattern, and the normal flux along one
 154 side of the control volume can be represented by the flux at the center of the side. The

155 finite volume discretization adopting the control volume as unit is depicted in Fig.1;
 156 the Gauss theorem can be followed for the integration of equation (8), wherein C_i
 157 represents the unit volume; after converting the volume integral flux function $F(V)$
 158 into the curved surface integral, we can obtain:

$$159 \quad \int_{C_i} \partial_i V dx + \oint_{\partial C_i} F(V) \cdot n_i d\sigma = \int_{C_i} G(V) dx \quad (9)$$

160 wherein, n_i represents the outward normal direction vertical to unit C_i at the
 161 boundary; through adopting the HLL format for the discretization of surface integral,
 162 the following simplified form can be obtained:

$$163 \quad V_i^{(*)} = V_i^{(n)} + \frac{\Delta t}{A_{C_i}} \Delta F_i^{(HLL)}(V^{(n)}) \quad (10)$$

$$164 \quad V_i^{(**)} = V_i^{(*)} + \frac{\Delta t}{A_{C_i}} \Delta F_i^{(HLL)}(V^{(*)}) \quad (11)$$

$$165 \quad V_i^{(n+1)} = \frac{1}{2} (V_i^{(n)} + V_i^{(**)}) \quad (12)$$

166 wherein, $V_i^{(n)}$ represents the mean value of unit variables at moment $t^{(n)}$; $V^{(n)}$
 167 represents the mean value of the entire grid at moment $t^{(n)}$; $\Delta t := t^{(n-1)} - t^{(n)}$ represents
 168 the calculated time step; A_{C_i} represents the area of unit C_i ; $\Delta F_i^{(HLL)}$ represents the
 169 approximate value of the curved surface integral, as shown below:

$$170 \quad \Delta F_i^{(HLL)}(V^{(n)}) := - \sum_{j=1}^4 F_{ij}^{(HLL)}(V^{(n)}) n_{ij} \Delta X \quad (13)$$

171 wherein, n_{ij} represents the outward normal direction of the i th unit at
 172 boundary j ; the flux calculation term $F_{ij}^{(HLL)}(V^{(n)})$ represents the approximate
 173 solution mode of the Riemann problem of the i th unit at boundary j ; see the
 174 computational formula below:

$$175 \quad F_{ij}^{(HLL)}(V^{(n)}) = \begin{cases} F(V_L^{(n)}) & 0 \leq S_L \\ \frac{S_R F(V_L^{(n)}) - S_L F(V_R^{(n)}) + S_R S_L F(V_R^{(n)} - V_L^{(n)})}{S_R - S_L} & S_L \leq 0 \leq S_R \\ F(V_R^{(n)}) & S_R \leq 0 \end{cases} \quad (14)$$

176 wherein, $V_L^{(n)}$ and $V_R^{(n)}$ respectively represent the approximate values of $V^{(n)}$

177 on both sides of boundary j of the i th unit; S_L and S_R respectively represent the
178 wave speeds on the left and right sides. Refer to the computational method described
179 by Toro (1992). In addition, the gradient magnitude in the original second-order
180 difference equation can be limited through multiplication with the flux limiter, and the
181 second-order format of the TVD property can be constructed to avoid the occurrence
182 of numerical oscillation. Refer to the specific method described by LeVeque (2002).

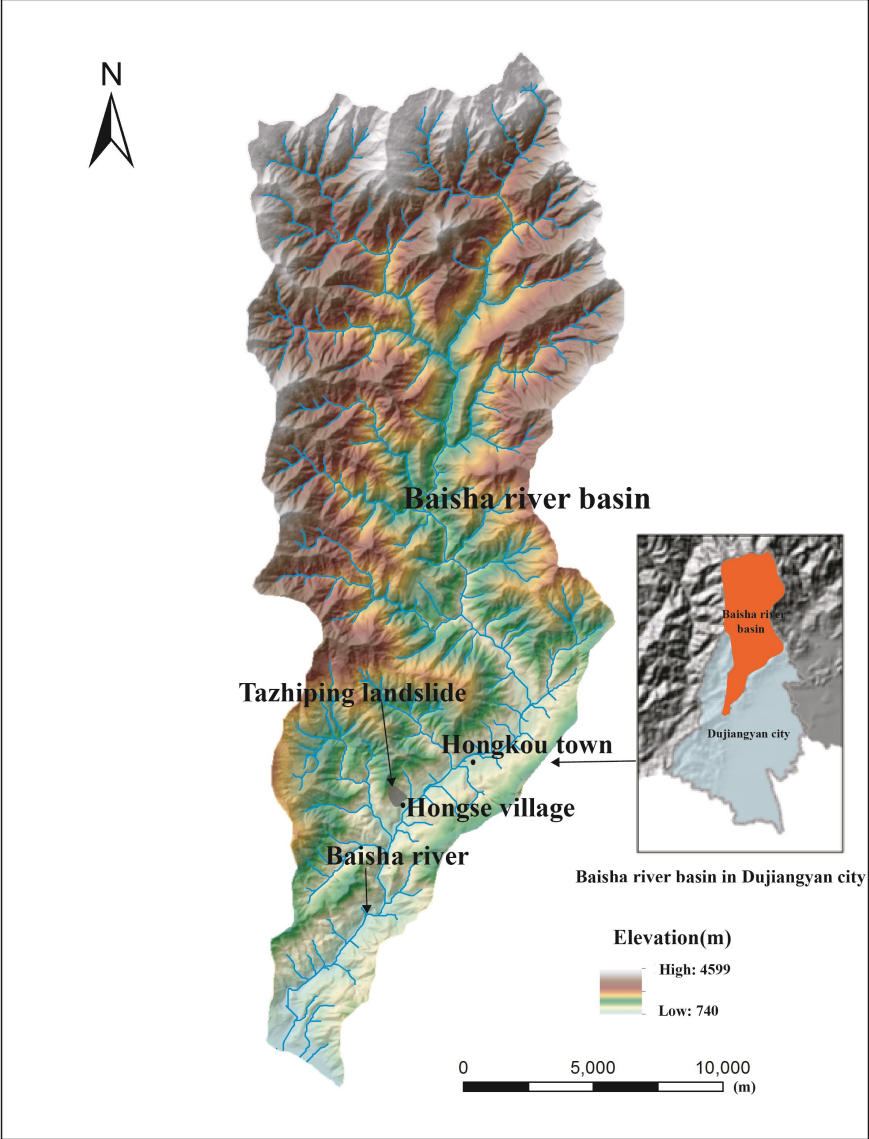
183 In this paper numerical solver used within RAMMS, which was specifically
184 designed to provide landslide(avalanche) engineers with a tool that can be applied to
185 analyze problems that two-dimensional depth-averaged mass and momentum
186 equations on three-dimensional terrain using both first and second-order finite volume
187 methods (Christen et al., 2010b).

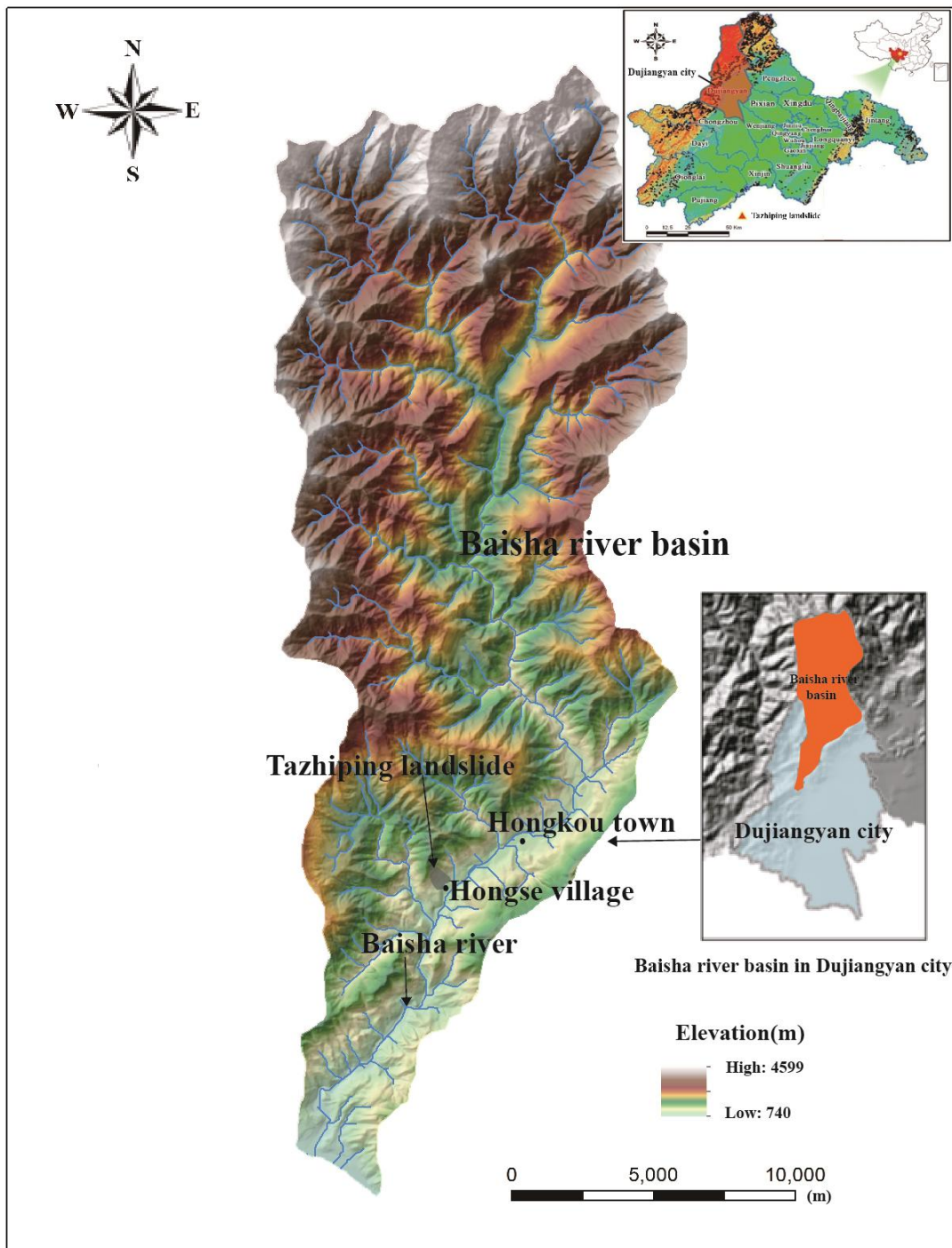
188 **3. Study area and data**

189 **3.1 Taziping landslide**

190 Taziping landslide is located in the southeast of the Hongse Village, Hongkou
191 Town, Dujiangyan City of Sichuan Province. The site is located at (E103°37'46",
192 N31°6'29"), 68 km away from Chengdu City to the east and 20 km away from the
193 Dujiangyan Urban District (Fig. 2). Its geomorphic unit is a middle-mountain tectonic
194 erosion area, falling within the slope geomorphology on the right bank of the Baisha
195 River Valley. As an colluvial layer landslide triggered by the Wenchuan Earthquake,
196 Taziping Landslide is a large-scale landslide as shown in Fig. 3. It has a gradient of
197 25°-40° with an average of about 32°. The landslide has an apparent round-backed
198 armchair contour, and has formed a steep rear edge, which has a gradient of 35°-50°
199 and an elevation of about 1,370 m. The front edge is located on the south side of the
200 mountain road, and has an elevation of about 1,007 m. The landslide has an elevation
201 difference of about 363 m, and the main sliding direction of 124°NE. The landslide
202 mass is in an irregular semi-elliptical shape, and has a length of about 530 m, an
203 average width of 145 m and a landslide area of approximately 7.68×10^4 m². The
204 landslide mass is gravelly soil in lithology, and is covered on the surface by silty clay
205 mingled with gravels. In terms of spatial distribution, it is thick in the middle and thin
206 on the lateral edges, and has a thickness of 20-25 m and a volume of approximately
207 1.16×10^6 m³. During the earthquake, the landslide mass slid to cover the northern
208 mountain slope mass of the Hongse Village Miaoba settlement. The landslide has an
209 apparent front edge boundary, and there is also a swelling deformation (Fig. 4).

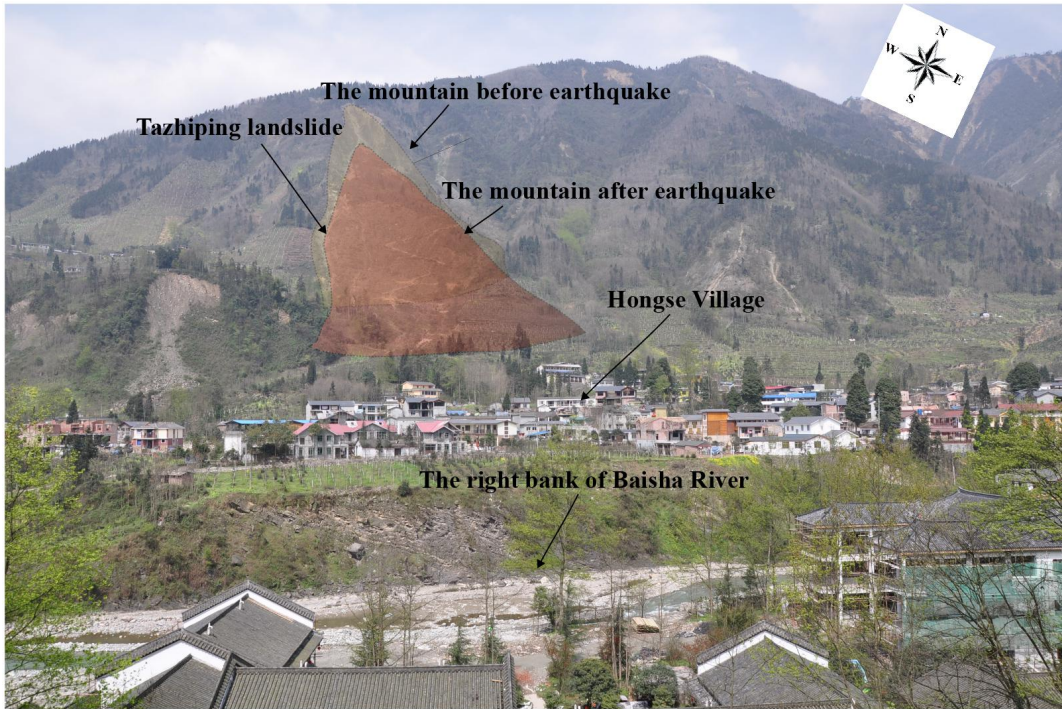
210





212
 213
 214

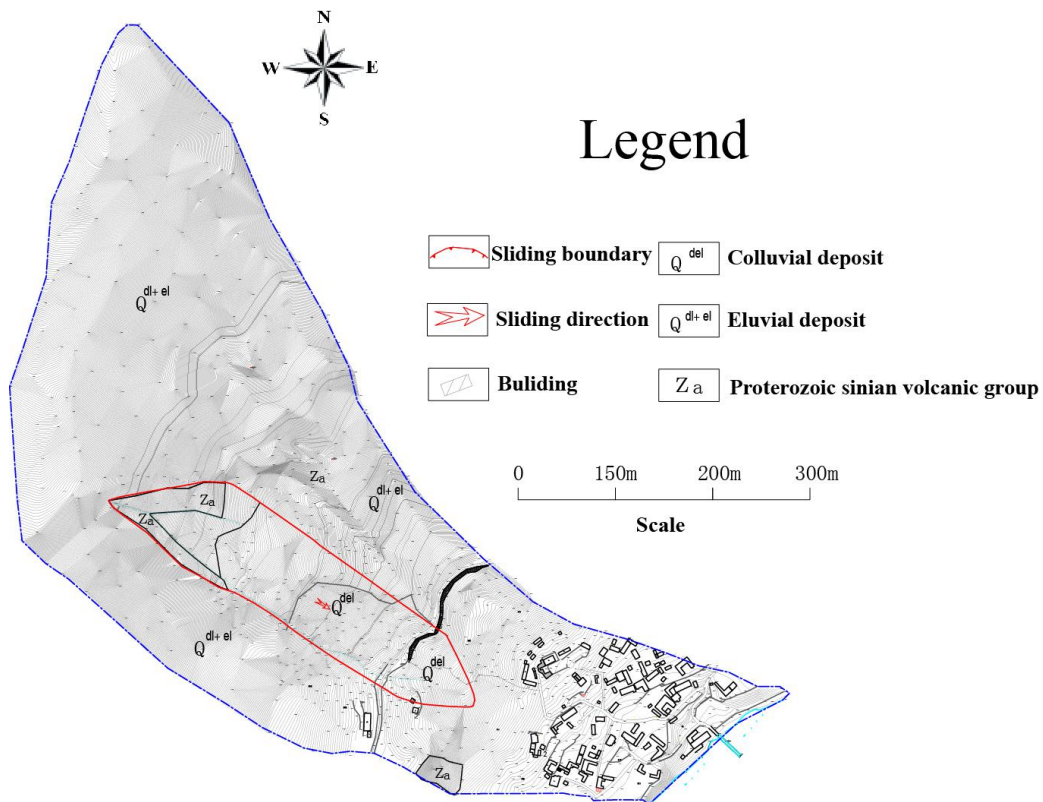
Fig.2 Location of Tazhiping landslide, Baisha river basin, Dujiangyan city (the landslide triggered by Wenchuan Ms 8.0 earthquake on May 12, 2008)



215

216

Fig.3 Tazhiping Landslide



217

218

Fig.4 Plane sketch of Tazhiping landslide

219

220

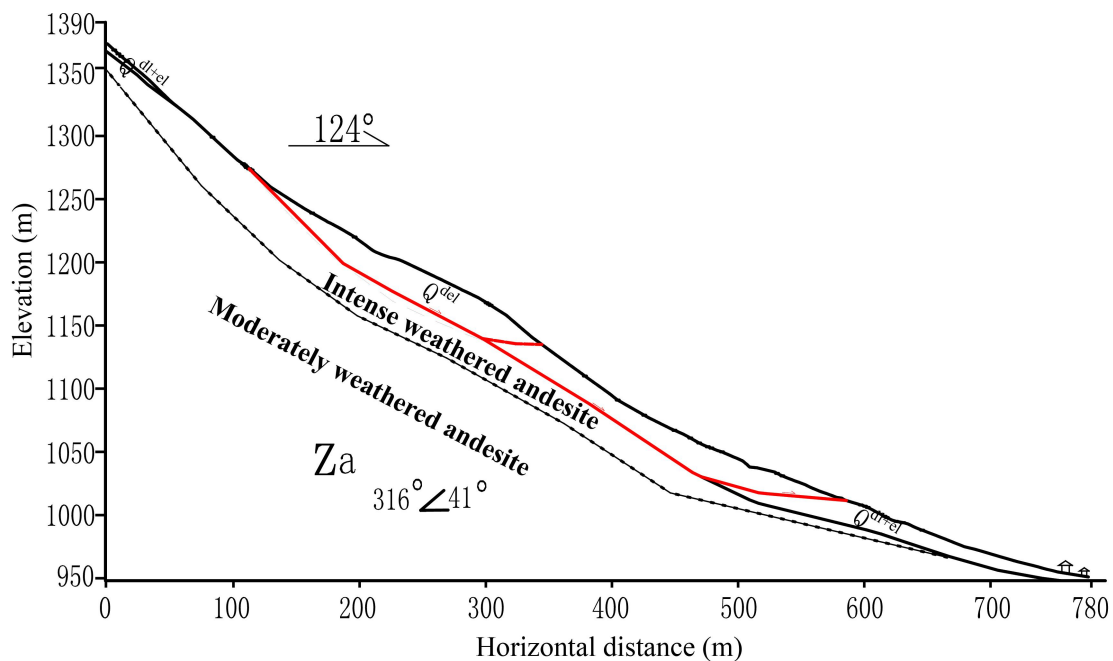
221

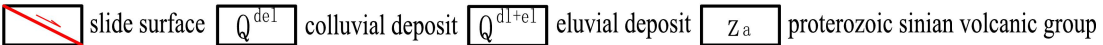
After Wenchuan Earthquake, the massive colluvial deposits covers on the mountain slope, and the landslide mass is dominated by the colluvium. The colluvium is mainly distributed on the top surface of the landslide mass in the thickness of

222 0.5-5.0 m, and is mainly constituted by rubbles and gravels. The mass consists of a
 223 small amount of fine gravel substances which are gray or grayish-green, and
 224 dominated by andesite in composition, generally with a block size of 20-150 cm.
 225 Field survey indicates that the rubbles in the surface layer have a maximum diameter
 226 exceeding 2 m, and that fine gravel substances are filled among rubbles in a loose
 227 structure. Within the thickness of 5-10 m, the landslide mass is constituted of a small
 228 amount of yellowish-brown and gray-brown silty clay mingled with 5-40% of
 229 non-uniformly distributed broken rubbles. Within the thickness of 10-25 m, there is a
 230 wide distribution of gravelly soil. The soil is grayish-green or variegated in color, is
 231 slightly compact and non-uniform, and has a broken stone content of about 50%. The
 232 parent rock of the broken stones is andesite, filled with silty clay or silt (Fig.4 5).
 233 Table 1 shows the parameters of the surface gravelly soil of the landslide mass based
 234 on the field sampling.

235 Tab.1 Parameters of the surface soil of Taziping Landslide

Internal friction angle (°)		Cohesion (kPa)	Relative compactness	Natural void ratio	Dry density (kN·m ⁻³)	Specific gravity (g·cm ⁻³)
Peak	Residual					
27.5	23	20.5	53%	0.789	15.357	2.492



236  237

238 Fig.4-5 Geological profile of Taziping Landslide

239 The landslide is an unconsolidated mass containing relatively large amounts of
 240 crushed stones and silty clay (Fig.5 6). Its loose structure and strong permeability
 241 facilitate infiltration of surface water. The Wenchuan earthquake aggravated the
 242 deformation of the landslide making deposits more unconsolidated, further reducing
 the stability of the landslide mass. During persistent rainfall, surface water infiltrates

243 the landslide slope resulting in increased water pressure within the landslide mass and
244 reduced shear strength on the sliding surface. Thus, rainfall constitutes the primary
245 inducing factor of the upper Taziping landslide. After infiltrating the loose layer, water
246 saturates the slope increasing the dead weight of the sliding mass and reducing the
247 shear strength of soil in the sliding zone. Infiltration into the landslide mass also
248 increases the infiltration pressure of perched water, drives deformation, and poses a
249 great threat to villages located at the front of the landslide. Slide-resistant piles and
250 backfill were placed at the toe of the slope in order to reduce the hazards of future
251 slides. The slide-resistant piles have enhanced the overall stability of the slope,
252 however, under heavy rainfall the upper unconsolidated landslide deposits may cut
253 out from the top of the slide-resistant piles.



254
255 (a) Material on the landslide surface (b) Material in the shear zone

256 Fig.5-6 Colluvial deposits covers on the mountain slope

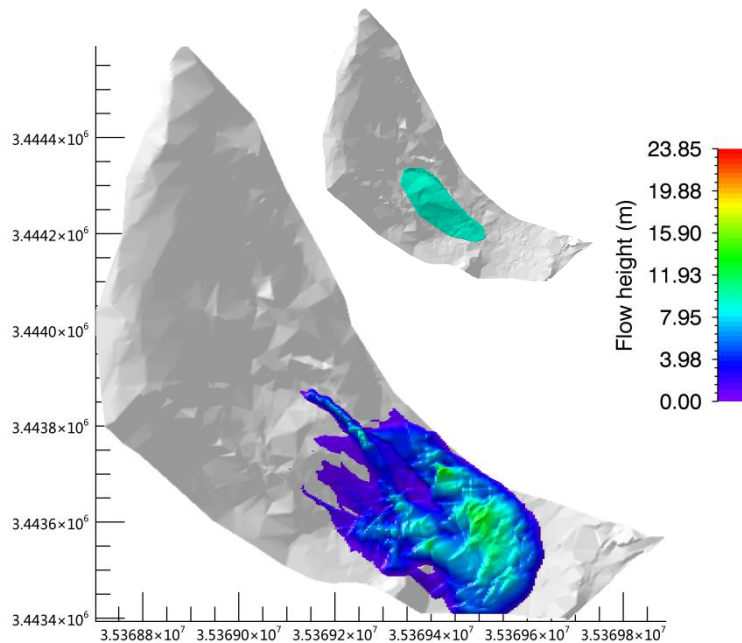
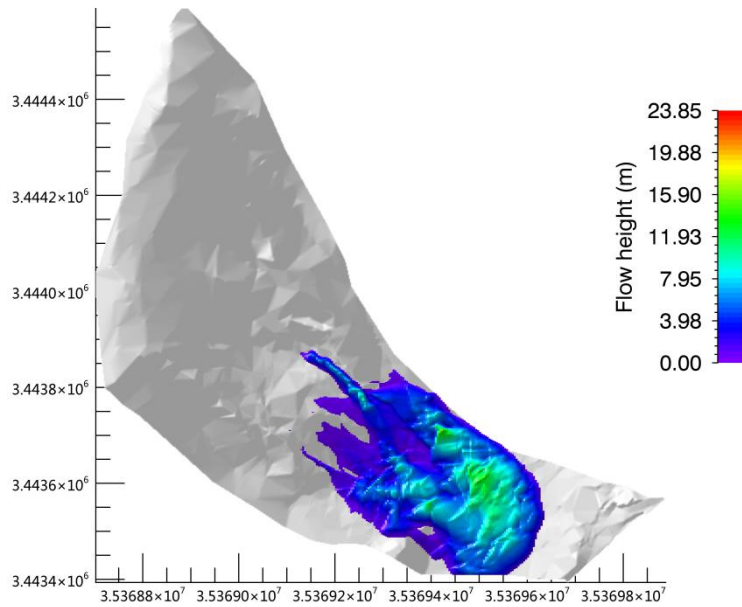
257 Therefore we simulate possible movement states of the Taziping landslide before
258 and after treatment with slide-resistant piles, comparatively analyzed the kinetic
259 parameters in the movement process, and mapped the 3D division of hazard zones.

261 3.2 Hazard prediction before treatment

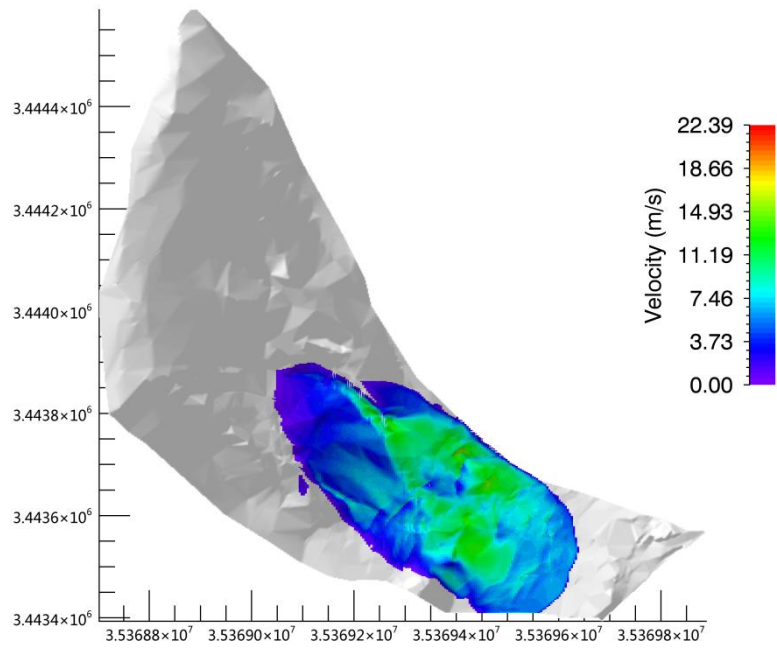
262 It was assumed that the landslide was damaged before engineering treatment.
263 According to field investigation, the sliding mass had an estimated starting volume of
264 about 600,000m³ and a mean thickness of 8m. Based on the survey report and field
265 investigation (Hydrologic Engineering and Geological Survey Institute of Hebei
266 Province, 2010), we adopted the survey parameters of Tab.2 for the simulated
267 calculation. These parameters obtained from performing laboratory or small-scale
268 experiments and back-analyses of relatively well-documented landslide cases. The
269 unit weigh $\gamma = 20.8kN \cdot m^{-3}$ which we used is from small-scale conventional
270 triaxial test experiments in laboratory. In addition, we selected the coulomb friction
271 coefficient $\mu = 0.45$ and viscous friction coefficient $\zeta = 500m \cdot s^{-2}$ in accordance
272 with back-analyses of well-documented landslide cases (Cepeda et al., 2010; Du et al.,
273 2015). The erosional entrainment rate selected the minimum value $k_i = 0.0001$ in
274 program RAMMS.

Tab.2 Model calculation parameters

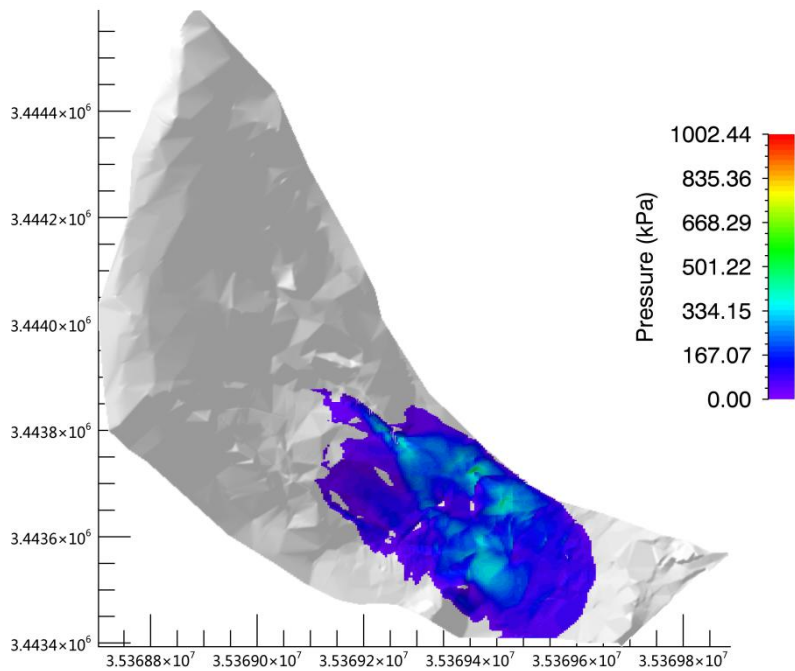
Unit weight $\gamma(kN \cdot m^{-3})$	Coulomb friction coefficient μ	Viscous friction coefficient $\zeta(m \cdot s^{-2})$	Erosional entrainment rate k_i
20.8	0.45	500	0.0001



(a) Thickness– Flow height



(b) Speed Velocity



(c) Pressure

Fig.67 Movement characteristic parameters of Taziping landslide (before treatment)

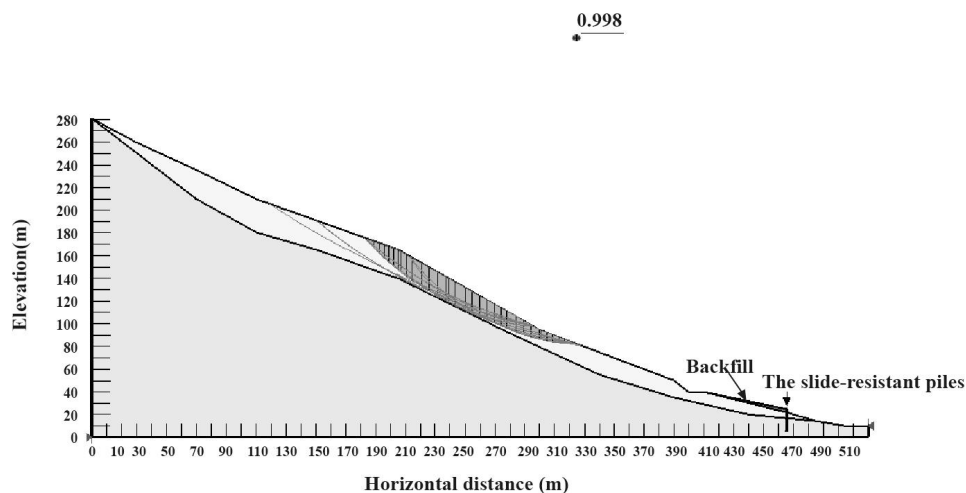
See the kinematic characteristic parameters of the landslide deposits in Fig.6 7. The colored bar shows the maximum values of moving process or an instantaneous for a given time step. As shown by the calculation results, \oplus deposits accumulated during the landslide movement process had a maximum thickness flow height of 23.85m, located around the surface gully of the middle and upper slope. The middle

289 and lower of the landslide deposits had a thickness flow height of about 5-10m; ②
 290 the middle and lower movement speed velocity of the landslide ranged from 3m/s and
 291 7m/s; ③ the landslide had a mean pressure of about 500kPa, and the pressure of the
 292 middle and lower deposits was about 200kPa. Thus, three-story and lower houses
 293 within the deposition range might be buried, and it was further suggested that the
 294 design strength of the gable walls of houses on the middle and upper parts of the
 295 deposit be increased above 300kPa.

296

297 3.3 Hazard prediction after treatment

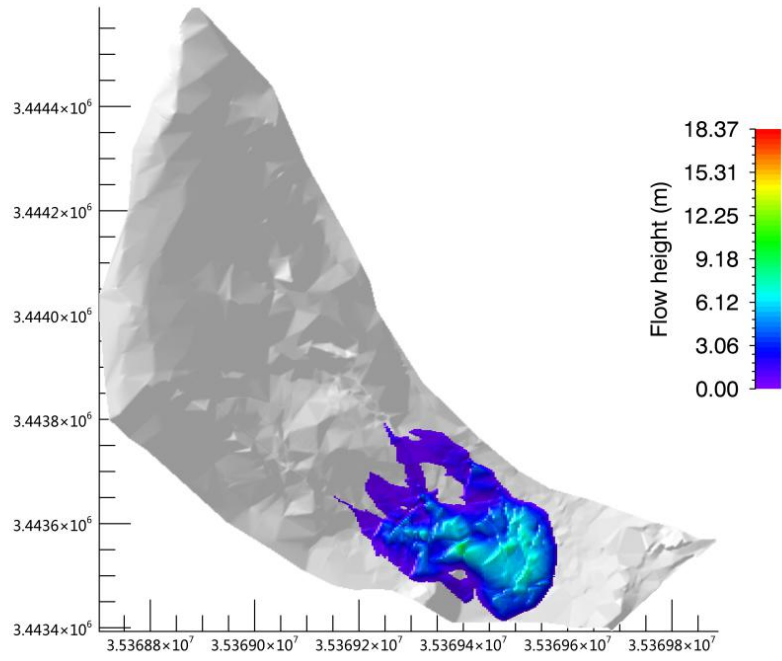
298 After fully accounting for the slide-resistant piles and mounds, we introduced the
 299 Morgenstern-Price method (Morgenstern et al., 1965) to calculate the stability
 300 coefficient of Taziping landslide after treatment. The method was determined with an
 301 iterative approaching by changing the position of the sliding surface until failure of
 302 the dumpsite (Fig.8). The physico-mechanical parameters under a saturated state
 303 (Hydrologic Engineering and Geological Survey Institute of Hebei Province, 2010)
 304 were adopted to search for the sliding plane of the landslide.



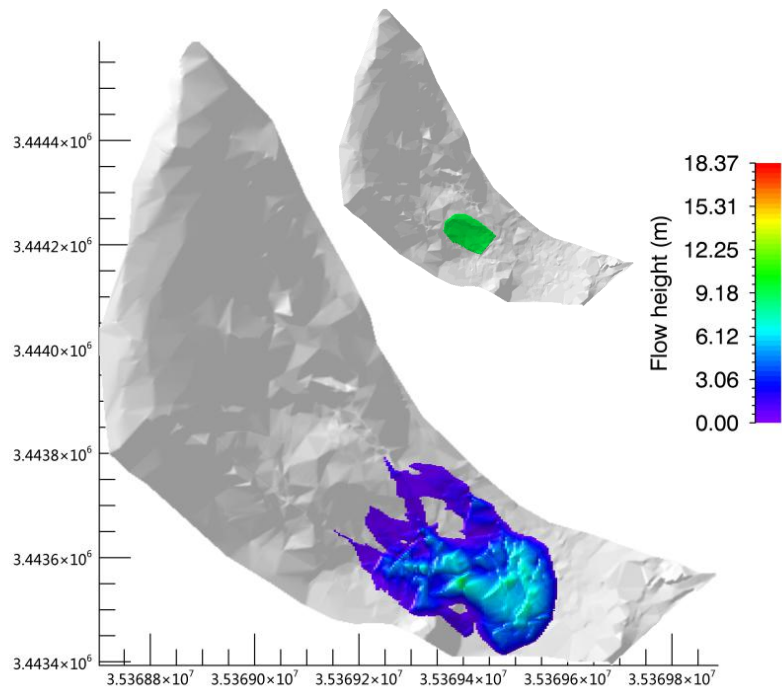
305

306 Fig.8 Search for the sliding plane of Taziping landslide (before treatment)

307 Based on the numerical analysis, the Taziping landslide stability coefficient was
 308 0.998. it was found under rainfall conditions, the middle area of Taziping landslide was
 309 unstable. Loose deposits in the middle part of the landslide might convert into
 310 high-water landslide substances and cut out from the top of the slide-resistant piles. In
 311 the damaged area, the slope had a rear edge wall elevation of about 1,170m. Its front
 312 edge was located on the south side of the mountain road, with an elevation of about
 313 ~~1,070m~~1,070-1,072m and a length of ~~about 180m~~182m. Thus, the scale of the
 314 rainfall-damaged is estimated to be about 250,000m³, with a mean thickness of about
 315 6m. The parameters in Tab.2 were again adopted for the simulated calculation.



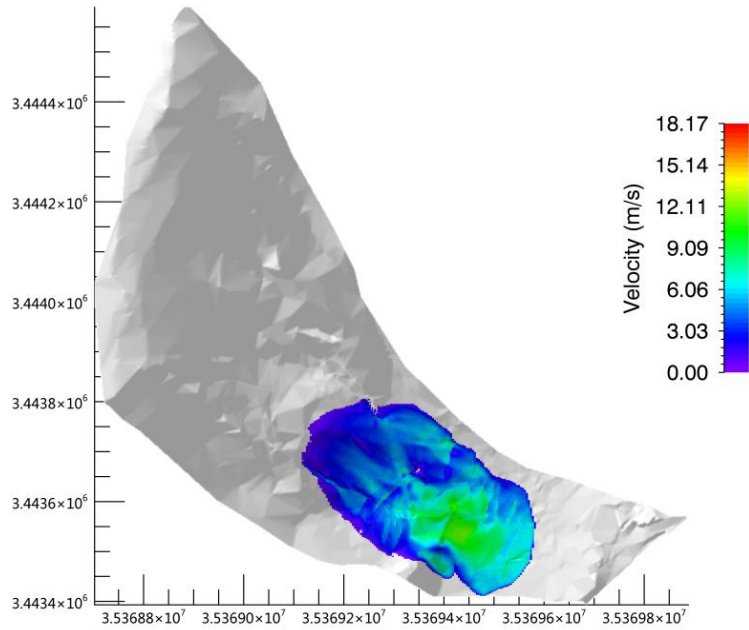
316



317

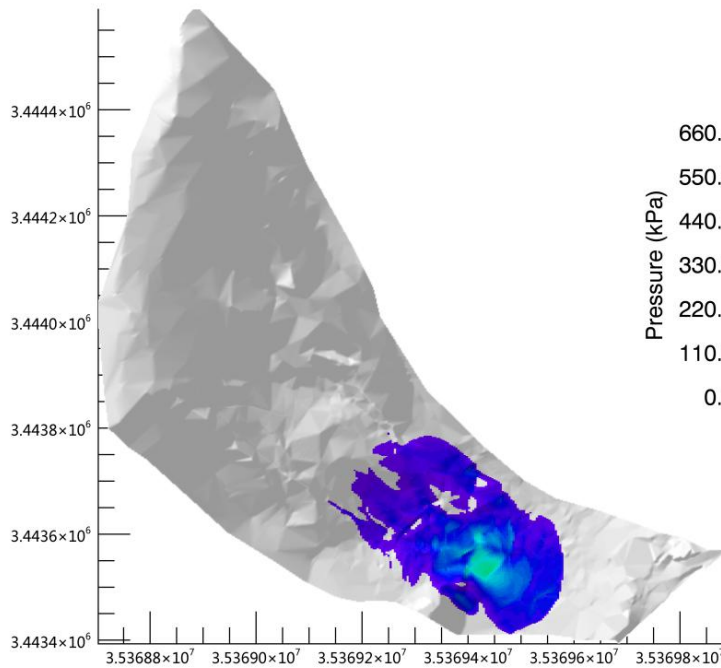
318

(a) Thickness– Flow height



319
320

(b) Speed Velocity



321
322

(c) Pressure

Fig.7 9 Movement characteristic parameters of Taziping landslide (after treatment)

Provided in Fig.4 9 are the kinematic characteristics of the landslide deposit. The coloredbar shows the maximum values of moving process or an instantaneous for a given time step. ①—Deposits accumulated during the landslide movement process had a maximum thickness flow height of 18.37m, located around the surface gully of the middle and upper slope. Middle and lower of the landslide deposits had a thickness flow height of approximately 3-5m. ②— The middle and lower movement-speed

330 **velocity** of the landslide deposits ranged between 3m/s and 5m/s. ③—The landslide
 331 had a mean pressure of about 330kPa, and the pressure of the middle and lower
 332 deposits was about 100kPa. Thus, it could be held that two-story and lower houses
 333 within the deposition range might be buried. It was further suggested that the design
 334 strength of the gable walls of houses on the middle and upper parts of the deposits be
 335 increased above 150kPa.

336 After treatment, the accumulation **thickness flow height** and pressure of the
 337 deposits were reduced by about 1/2, and the kinematic speed was reduced by about
 338 1/3. However, the Miaoba residential area of Red Village was still partially at hazard.
 339

340 **4 Results**

341 **Landslides reflect landscape instability that evolves over meteorological and**
 342 **geological timescales, and they also pose threats to people, property, and the**
 343 **environment. The severity of these threats depends largely on landslide speed and**
 344 **travel distance. There may be examples where entire houses on a landslide mass are**
 345 **moved but not destroyed because of stable base plates. In any case, velocity plays a**
 346 **more important role regarding kinetic energy acting on an obstacle. However, the**
 347 **Miaoba residential area of Red Village is located at the frontal part of Tazhiping**
 348 **lanslide. Then, D**uring landslide movement, the spatial scale indexes of a landslide
 349 mass include area, volume, and thickness. The maximum thickness of the landslide is
 350 one of the direct factors influencing the building’s deformation failure status. A large
 351 landslide displacement may lead to burial, collapse, or deformation failure of the
 352 building, and thus influence its safety and stability. Thus, landslide thickness
 353 constitutes an important index for assessing the hazards of a landslide disaster, and for
 354 influencing the consequences faced by disaster-affected bodies (Fell et al., 2008;
 355 DZ/T, 0286-2015). Provided in Tab.3 is a landslide thickness-based division of the
 356 predicted hazard zones of Taziping landslide, in which the thickness of the landslide
 357 mass correlates with the ability of a building to withstand a landslide disaster (Hung
 358 et al., 1984; Petrazzuoli et al., 2004; GB, 50010–2010; Hu et al., 2012; Zeng et al.,
 359 2015). After treatment with slide-resistant piles, the hazard of a future slide was
 360 reduced by about 1/3 overall and by 2/3 in high-hazard zones.

361 **Tab.3 Division table of the predicted hazards of Taziping landslide (unit: m²)**

Hazard zone level	Assessment index	Building damage probability	Area before treatment	Area after treatment	Increased/decreased area	Building damage characteristics
Low-hazard zone						One-story houses
(I)	$h \leq 0.5m$	20%	44 , 600	38 , 748	-5,852	may be damaged; houses on the

						landslide mass are partially damaged.
						One-story houses have a very high probability of being
Relatively low-hazard zone (II)	$0.5 \text{ m} < h \leq 1 \text{ m}$	50~20%	24 , 900	26 , 400	+1,500	washed-away damaged; one-story houses on the landslide mass are completely damaged.
						One-story to three-story houses have a very high probability of being
Moderate-hazard zone (III)	$1 \text{ m} < h \leq 3 \text{ m}$	80~50%	21 , 980	15 , 856	-6,124	washed-away damaged; houses less than three stories on the landslide mass are completely damaged.
						One-story houses may be buried, and
Relatively high-hazard zone (IV)	$3 \text{ m} < h \leq 5 \text{ m}$	100~80%	30 , 820	19 , 636	-11,184	two-story to six-story houses have a very high probability of being
						washed-away

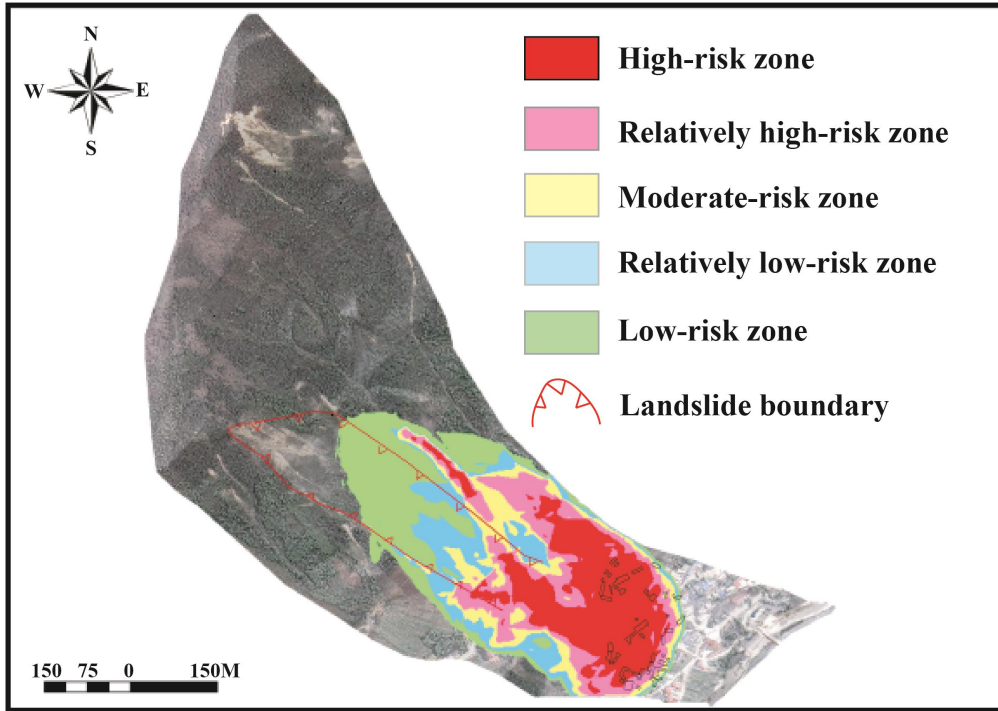
High-hazard

zone	$h \geq 5m$	100%	47 , 240	13 , 052	-34,188
(V)					

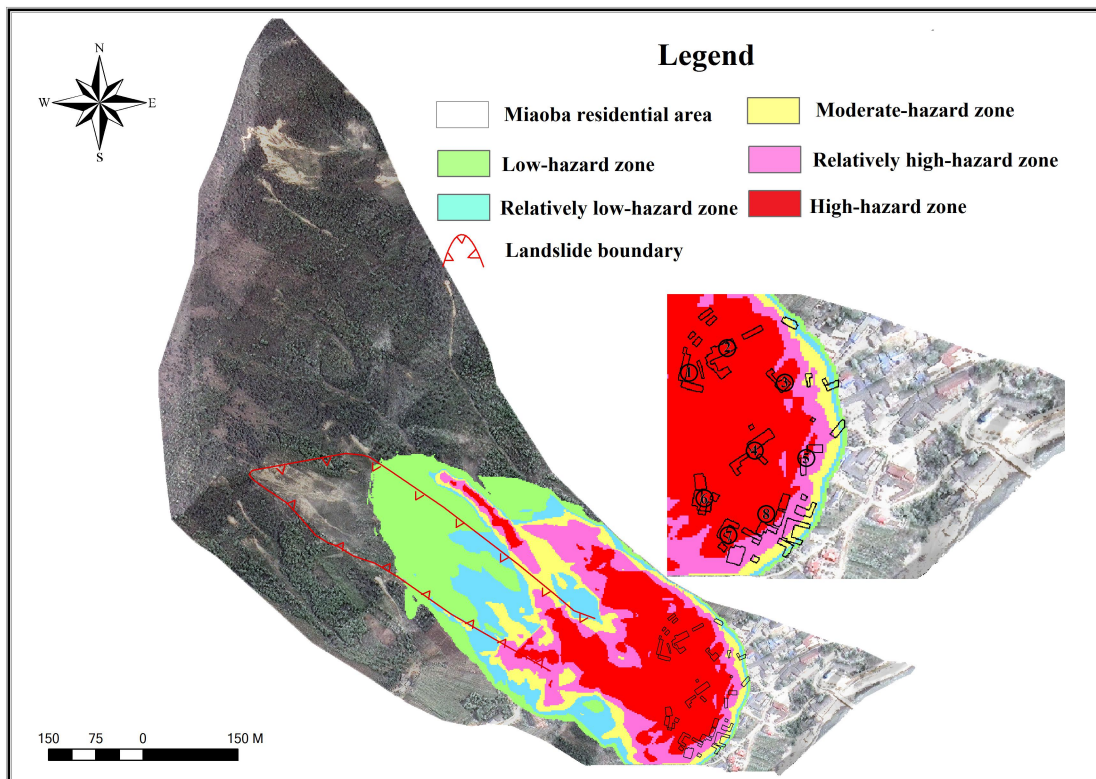
Total area:	—	—	169 , 540	113 , 700	-54,340	—
-------------	---	---	-----------	-----------	---------	---

damaged; houses on the landslide mass are completely damaged. Two-story and lower houses may be buried, and three-story and higher houses have a very high probability of being washed away damaged; houses on the landslide mass are completely damaged.

362 Given in Fig.8 10 are the 3D divisions of hazard zones of Taziping landslide
 363 before and after engineering treatment. The scope of the hazard zones changed before
 364 and after engineering treatment, particularly in the high-hazard zones. Before
 365 treatment with slide-resistant piles, the landslide posed a great hazard to eight houses
 366 on the left side of the upper Miaoba residential area, with high-hazard zone associated
 367 with landslide mass height over 5m and red zone. After treatment, the number of
 368 effected houses was reduced to four. We defined outside the colored area as
 369 no-hazard.



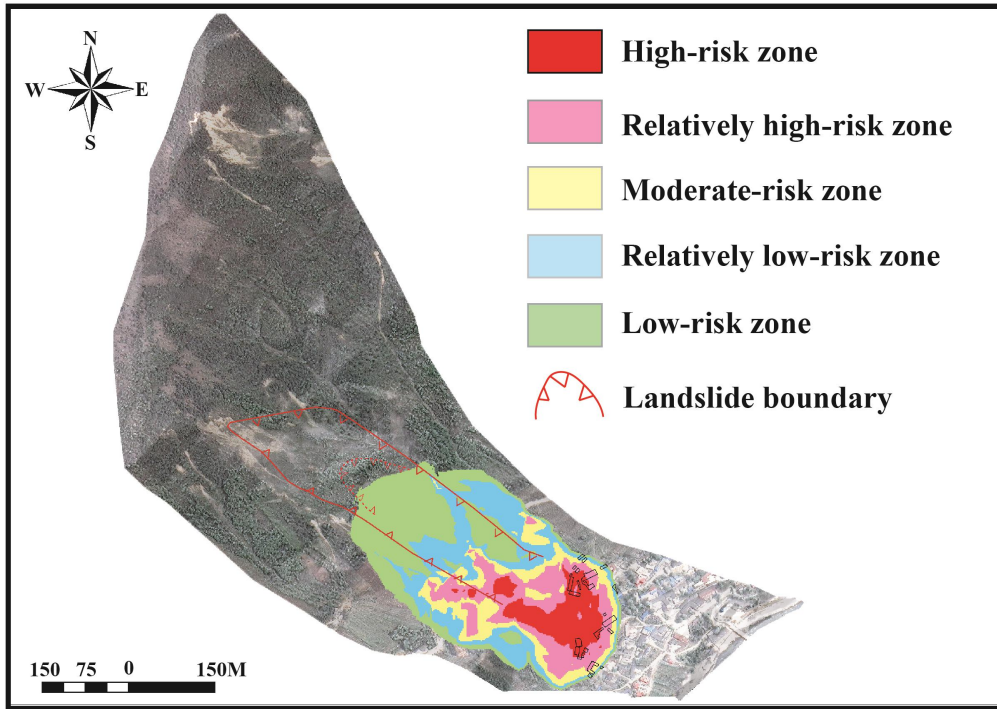
370



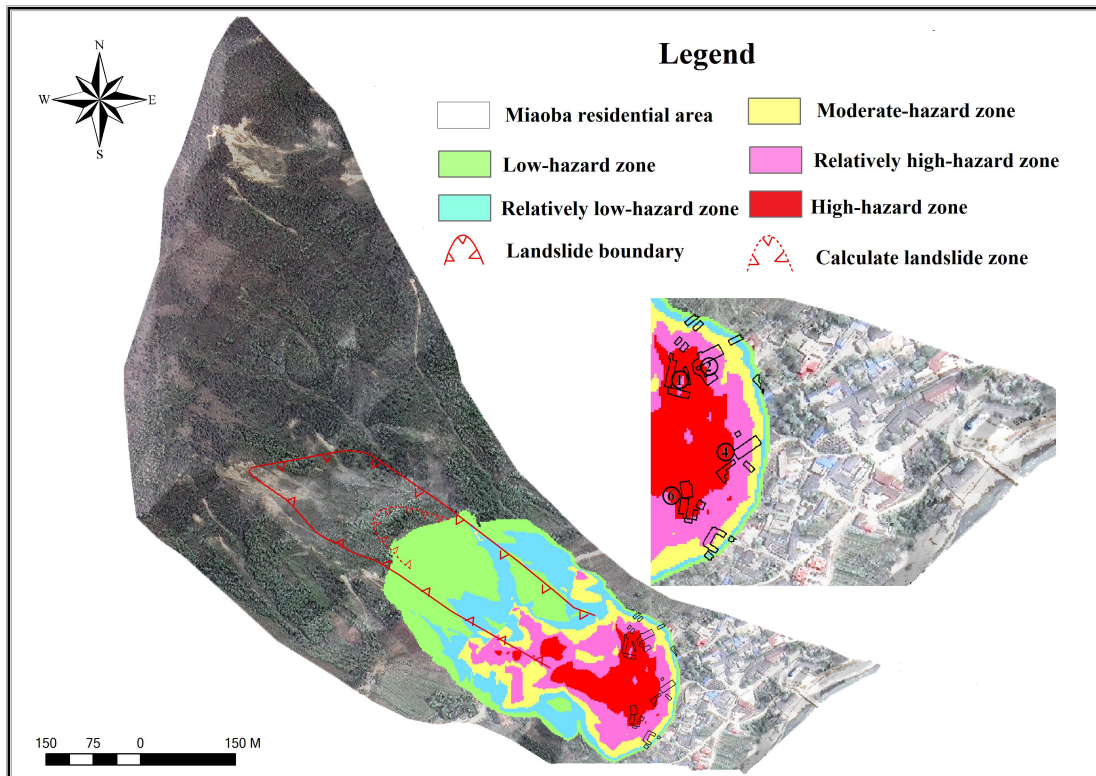
371

372

(a) Before treatment



373



374

375

(e) After treatment

376

Fig.810 3D division comparison of the hazards of Taziping landslide

377

378 5 Conclusions and Discussion

379

The hazard assessment of landslide using numerical models is becoming more and more popular as new models developing and becoming available in both scientific

380

381 research and practical applications. There is some confusion about the mass
382 movement process that is discussed and approached by the presented and adopted
383 rheological model.

384 On the one hand, Landslides move downslope in many different ways (Varnes,
385 1978). In addition landslides can evolve into rapidly travelling flows, which exhibit
386 characteristics of debris flows on unchannelized or only weakly channelized hillslopes.
387 The geomorphic heterogeneity of rapid shallow landslides such as hillslope debris
388 flows is larger than observed in channelized debris flows, however many of these
389 flows can be successfully modelled using the Voellmy-fluid friction relation and
390 starting the flow as a block release (Christen et al., 2012). This paper simulation
391 results support this option that Voellmy-fluid rheological model can also be used in
392 the simulation of flow-type landslides.

393 On the other hand, The selection of model parameters remains one of the
394 fundamental challenges for numerical calculations in natural hazards. At present, there
395 are a high empirical parameters obtained from 30-year monitoring data on avalanche.
396 Such as in RAMMS, we can automatically generate the friction coefficient of
397 avalanche for our calculation domain based on topographic data analysis, forest
398 information and global parameters and so on (WSL, 2013). The friction parameters of
399 debris flow can found in some literature (Fannin et al., 2001; Iovine et al., 2003;
400 Hürlimann et al., 2008; Scheidl et al., 2010; Huang et al., 2015). However, There are
401 seldom cases researching on friction parameters of flow-type landslide. Therefore, we
402 tested different coulomb friction coefficient μ values ranging between $0.1 \leq \mu \leq 0.6$

403 and viscous friction coefficient ζ values ranging between $100 \leq \mu \leq 1000 m \cdot s^{-2}$.

404 Finally, we selected the coulomb friction coefficient $\mu = 0.45$ and viscous friction
405 coefficient $\zeta = 500 m \cdot s^{-2}$ in accordance with back-analyses of well-documented
406 landslide cases (Cepeda et al., 2010; Du et al., 2015). The results of the simulation
407 results is consistent with the field observation in terms of topography and sliding path.

408 Based on the finite volume method and program RAMMS, the simulation results
409 of Taziping landslide were consistent with the sliding path predicted by the field
410 investigation. This correlation indicates that numerical simulation is an effective
411 method for studying the movement processes of flow-type landslide-debris flows. The
412 accumulation thickness flow height and pressure of landslide deposits were reduced
413 by about 1/2, and the kinematic speed was reduced by about 1/3 after treatment.
414 However, the Miaoba residential area of Red Village is still partially at hazard.
415 Considering that two-story and lower houses within the deposition range might be
416 buried, it was further suggested that the design strength of the gable walls of houses
417 on the middle and upper parts of the deposit be increased above 150kPa.

418 By utilizing a GIS platform in combination with landslide hazard assessment
419 indexes, we mapped the 3D division of the Taziping landslide hazard zones before
420 and after engineering treatment. The results indicated that overall hazard zones

421 contracted after engineering treatment and, the area of high-hazard zones was reduced
422 by about 2/3. After engineering treatment, the number of at hazard houses on the left
423 side of the upper Miaoba residential area, was reduced from eight to four. It was thus
424 clear that some zones are still at high hazard despite engineering treatment. Therefore,
425 it was proposed that houses located in high-hazard zones be relocated or reinforced
426 for protection.

427

428

429

430 **Acknowledgments**

431 First of all, the authors give sincere acknowledgement to CAS Pioneer Hundred
432 Talents Program for the completion of this research. Also this work was supported by
433 National Natural Science Foundation of China (Grant No. 41301009) and the
434 Hundred Young Talents Program of IMHE (SDSQB-2016-01), the International
435 Cooperation Program of the Ministry of Science and Technology of China (Grant
436 No.2013DFA21720). The authors express their deepest gratitude to those aids and
437 assistances. **The authors also extend their gratitude to editor and two anonymous**
438 **reviewers for their helpful suggestions and insightful comments, which have**
439 **contributed greatly in improving the quality of the manuscript.**

440

441

442 **Reference**

443 Bartelt, P., Bühler, Y., Buser, O., Christen, M., and Meier, L.: Modeling mass-dependent flow
444 regime transitions to predict the stopping and depositional behavior of snow avalanches, *J.*
445 *Geophys. Res.*, 117, F01015, doi:10.1029/2010JF001957, 2012 .

446 Costa, J.E.: Physical geomorphology of debris flows. *Developments and Applications of*
447 *Geomorphology*, Springer Press., 268-317, 1984.

448 Christen, M., Kowalski, J., and Bartelt, P.: RAMMS: Numerical simulation of dense snow
449 avalanches in three-dimensional terrain, *Cold Regions Science and Technology.*, 63, 1–14,
450 2010.

451 Christen, M., Bartelt, P., and Kowalski, J.: Back calculation of the In den Arelen avalanche with
452 RAMMS: interpretation of model results, *Annals of Glaciology.*, 51, 161–168, 2010.

453 **Christen, M., Bühler, Y., Bartelt, P., Leine, R., Glover, J., Schweizer, A., Graf, C., McArdell, B.,**
454 **Gerber, W., Deubelbeiss, Y., Feistl, T., and Volkwein, A.: Integral hazard management using a**
455 **unified software environment: numerical simulation tool “RAMMS” for gravitational natural**
456 **hazards, In: Koboltschnig, G., Hübl, J., Braun, J. (eds.) Proceedings of 12th Congress**
457 **INTERPRAE., 1, 77–86, 2012.**

458 **Chen, J.C., and Chuang, M.R.: Discharge of landslide-induced debris flows: case studies of**
459 **Typhoon Morakot in southern Taiwan, *Nat. Hazards Earth Syst. Sci.*, 14, 1719-1730, 2014.**

460 **Cepeda, J., Chávez, J.A., and Martínez, C.C.: Procedure for the selection of runout model**
461 **parameters from landslide back-analyses : application to the Metropolitan Area of San**
462 **Salvador, El Salvador, *Landslides.*, 7, 105–116, 2010.**

463 Du, J., Yin, K.L., and Wang, J.J.: Simulation of three-dimensional movement of landslide-debris

464 flow based on finite volume method, *Chinese Journal of Rock Mechanics and Engineering.*,
465 34: 480–488, 2015 (in Chinese).

466 Evans, S.G., Tutubalina, O.V., Drobyshev, V.N., Chernomorets, S.S., McDougall, S., Petrakov,
467 D.A., and Hungr, O.: Catastrophic detachment and high-velocity long-runout flow of Kolka
468 Glacier, Caucasus Mountains, Russia in 2002, *Geomorphology.*, 105, 314–321, 2009.

469 Fannin, R.J., and Wise, M.P.: An empirical-statistical model for debris flow travel distance,
470 *Canadian Geotechnical Journal.*, 38, 982–994, 2001.

471 Finlay, P.J., Mostyn, G.R., and Fell, R.: Landslide risk assessment: prediction of travel distance,
472 *Canadian Geotechnical Journal.*, 36, 556–562, 1999.

473 Fell, R., Corominas, J., Bonnard, C., Cascini, L., Leroi, E., and Savage, W. Z.: Guidelines for
474 landslide susceptibility, hazard and risk zoning for land use planning, *Engineering Geology.*,
475 102, 85–98, 2008.

476 Fannin, R., and Wise, M.: An empirical-statistical model for debris flow travel distance, *Can*
477 *Geotech J.*, 38, 982–994, 2001.

478 GB 50010–2010.: Code for design concrete structures, Beijing: Chinese Architectural Industry.,
479 34–80, 2010 (in Chinese).

480 Hebei Province Institute of Hydrogeological and Engineering.: Geological investigation
481 engineering supplemental survey report of Hongse Village Taziping landslide in Hongkou
482 Town of Dujiangyan City, Sichuan Province., 2010 (in Chinese).

483 Hungr, O.: A Model for the runout analysis of rapid flow slides, debris flows and avalanches, *Can*
484 *Geotech J.*, 32, 610–623, 1995.

485 Hungr, O., Evans, S.G., Bovis, M.J., and Hutchinson, J.N.: A review of the classification of
486 landslides of the flow type, *Environ Eng Geosci.*, 7, 221–238, 2001.

487 Hungr, O., Morgan G.C., and Kellerhals, R.: Quantitative analysis of debris torrent hazards for
488 design of remedial measures, *Can Geotech J.*, 21, 663–677, 1984.

489 Hu, K.H., Cui, P., and Zhang, J.Q., Characteristics of damage to buildings by debris flows on 7
490 August 2010 in Zhouqu, Western China, *Nat Hazards Earth Syst Sci.*, 12, 2209–2217, 2012.

491 Hürlimann, M., Rickenmann, D., Medina, V., and Bateman, A.: Evaluation of approaches to
492 calculate debris-flow parameters for hazard assessment, *Eng Geol.*, 102, 152–163, 2008.

493 Huang, Y., Cheng, H., Dai, Z., Xu, Q., Liu, F., Sawada, K., Moriguchi, S., and Yashima, A.:
494 SPH-based numerical simulation of catastrophic debris flows after the 2008 Wenchuan
495 earthquake, *Bull Eng Geol Environ.*, 74, 1137–1151, 2015.

496 Iverson, R. M., Reid, M. E., and LaHusen, R. G.: Debris-flow mobilization from landslides, *Annu.*
497 *Rev. Earth Planet Sc.*, 25, 85– 138, 1997.

498 Iverson, R.M., and Vallance, J.W.: New views of granular mass flows, *Geology.*, 29, 1115–1118,
499 2001.

500 Iovine, G., Gregorio, S.D., and Lupiano, V.: Debris-flow susceptibility assessment through cellular
501 automata modeling: an example from 15–16 December 1999 disaster at Cervinara and San
502 Martino Valle Caudina (Campania, southern Italy), *Nat Hazards Earth Syst Sci.*, 3, 457–468,
503 2003.

504 Jackson, L.E., Kostashuk, R.A., and MacDonald, G.M.: Identification of debris flow hazard on
505 alluvial fans in the Canadian Rocky mountains, *Geological Society of America.*, 7, 155–124,
506 1987.

507 LeVeque, R.: *Finite Volume Methods for Hyperbolic Problems*, Cambridge Texts in Applied

508 Mathematics Cambridge University Press., 2002.

509 ~~Michael, L.M., 2003. Baynes F, Scott G, Granger K Regional landslides risk to the Cairns~~
510 ~~community[J]. Nat Hazards, 2003, 30 (2): 233-249.~~

511 Michael-Leiba, M., Baynes, F., Scott, G., and Granger, K.: Regional landslides risk to the Cairns
512 community, Nat Hazards., 30, 233–249, 2003.

513 Morgenstern, N.R., and Price, V.E.: The analysis of the stability of general slip surfaces,
514 Geotechnique., 15, 79–93, 1965.

515 Portilla, M., Chevalier, G., and Hürlimann, M.: Description and analysis of the debris flows
516 occurred during 2008 in the Eastern Pyrenees, Nat. Hazards Earth Syst. Sci., 10, 1635–1645,
517 2010.

518 Petrazzuoli, S.M., and Zuccaro, G.: Structural resistance of reinforced concrete buildings under
519 pyroclastic flows: a study of the Vesuvian area, J Volcanol Geoth Res., 133, 353–367, 2004.

520 Sassa, K., Nagai, S., Solidum, R., Yamazaki, Y., and Ohta, H.: An integrated model simulating the
521 initiation and motion of earthquake and rain induced rapid landslides and its application to
522 the 2006 Leyte landslide, Landslides., 7, 219–236, 2010.

523 Scott, K.M., and Vallance, J.W.: History of Landslides and Debris Flows at Mount Rainier: Water
524 Fact Sheet, USGS Open-File Report., 93–111, 1993.

525 Shi, G.H.: Discontinuous deformation analysis - a new numerical model for the statics and
526 dynamics of block system, Berkeley: University of California., 1988.

527 ~~DZ/T 0286-2015.: Specification of risk assessment for geological hazard, Ministry of Land and~~
528 ~~Resources of the People's Republic of China., 2015 (in Chinese).~~

529 Scheidl, C., and Rickenmann, D.: Empirical prediction of debris-flow mobility and deposition on
530 fans, Earth Surf Proc Land., 35, 157–173, 2010.

531 Toro, E.F.: Riemann problems and the waf method for solving the two dimensional shallow water
532 equations. Philos. Trans. R. Soc. London., Ser. A 338, 43–68, 1992.

533 Varnes, D.J., : Slope movement types and processes. In: Schuster RL, Krizek RJ (eds) Landslides:
534 analysis and control. Transportation Research Board, National Research Council, Washington,
535 DC, USA., 11–33 , 1978.

536 Wang, L., Li, B., Gao, Y., and Zhu, S.: Run-out prediction of large thick-bedded unstable rock: A
537 case study of Daxiang unstable rock in Yangjiao town, Wulong county, Chongqing, Earth
538 Science Frontiers., 23, 251–259, 2016 (in Chinese).

539 WSL.: RAMMS: A numerical model for snow avalanches in research and practice, User manual
540 v1.5 avalanche, WSL Institute for snow and avalanche research SLF, Swiss., 2013.

541 ~~Yin, K.L., Jiang, Q.H., and Wang, Y.: Simulation of Landslide Movement Process by~~
542 ~~Discontinuous Deformation Analysis, Earth Science Journal of China University of~~
543 ~~Geosciences, 27, 632-636, 2002 (in Chinese).~~

544 ~~Zhang, Y.J.: Study on dynamic characteristics of typical rock avalanche on canyon area, Shanghai~~
545 ~~Jiao Tong University, 2013 (in Chinese).~~

546 ~~Zhang, Z.Y., Wang, S.T., Wang, L.S., Huang, R.Q., Xu, Q., and Tao, L.J.: Principles of~~
547 ~~engineering geology, Beijing: Geology Press., 212-224, 1993 (in Chinese).~~

548 Zeng, C., Cui, P., Su, Z.M., Lei, Y., Chen, R.: Failure modes of reinforced concrete columns of
549 buildings under debris flow impact, Landslides., 12, 561-571, 2015.